Biosensors and Bioelectronics 134 (2019) 24–28

Contents lists available at ScienceDirect

Biosensors and Bioelectronics

journal homepage: www.elsevier.com/locate/bios

Glucose oxidase mimicking half–sandwich nickel(II) complexes of coumarin substituted N–heterocyclic carbenes as novel molecular electrocatalysts for ultrasensitive and selective determination of glucose

K.N. Brinda[a], Gautam Achar[a], Jan Grzegorz Małecki[b], Srinivasa Budagumpi[a,*], D.H. Nagaraju[a,**], V. Suvina[a], R. Geetha Balakrishna[a]

[a] Centre for Nano and Material Sciences, Jain University, Jain Global Campus, Kanakapura, Ramanagaram, Bangalore, 562112, India
[b] Department of Crystallography, Institute of Chemistry, University of Silesia, 9th Szkolna St., 40–006, Katowice, Poland

ARTICLE INFO

Keywords:
Electro–oxidation
Non enzymatic glucose sensor
Half–sandwich Ni complex
Imidazolium salt
N–heterocyclic carbene

ABSTRACT

Glucose oxidase mimicking nickel–based porous structures with organic anchors are developed as cheap and reliable electrochemical sensors for the quantitative detection of glucose. A series of sterically and electronically modulated, air– and moisture–stable half–sandwich nickel(II) NHC complexes were prepared and characterized. Under the optimized electrocatalytic conditions, the nickel complex immobilized glassy carbon electrodes (GCEs) displayed high sensitivity (0.663, 1.280, 1.990 and 0.182 μA/μM) towards glucose detection, which is much higher than that of 3D porous nickel networks. The limit of detection of modified GCEs is found in the range 1.56–2.09 μM with much wider linear sensing range, and having a catalytic rate constant of $0.273 \times 10^3\,M^{-1}s^{-1}$. Finally, the selectivity of the modified GCEs towards glucose in presence of other blood constituents was also evaluated.

1. Introduction

The first enzyme based biosensor was designed, patented and commercialized by Clark and Lyons in the year 1962 (Clark and Lyons, 1962), which consist the enzyme, glucose oxidase, coupled with signal transducers that can behave as glucose sensors. However, they carry disadvantages pertaining to the electrochemical response and denaturation of the enzyme (Wang and Zhuang, 2017). The non–enzymatic glucose sensors have been fabricated with an intension to address the drawbacks pertaining to enzymatic sensors. It is however, essential to design and fabricate cost–effective, stable, robust and sensitive non–enzymatic electrochemical sensor, which mimic the functions of glucose oxidase enzyme. Off late, nanomaterial supported metal and metal oxides have been largely explored, particularly, bulk nickel and nickel nanoparticles–based electrocatalytic materials displayed promising sensing abilities (Niu et al., 2016). However, a major disadvantage of using a nanocatalyst is its quantification and poor selectivity. A molecular catalyst, on the other hand, is quantifiable and more importantly the uniform modification of the electrode is possible using its homogenous solution. In this regard, NHC complexes in particular have been used as electrochemical sensors (Prathap et al., 2013), while their structures can be fine–tuned to further improve the catalytic efficiency. In spite of having significant advantage of being cheap, easy to prepare and convenient to be used as catalysts, Ni(II)—NHC complexes are relatively less explored. This work–gap motivated us to pioneer the work involving CpNi(II)—NHC complexes as possible electrocatalysts.

2. Results and discussion

2.1. Synthesis and characterization of imidazolium salts and CpNi–NHC complexes

Mesityl and coumarin substituted imidazolium bromide salts, **4**, **5**, **10** and **11**, were prepared conventionally by the reaction of 1–mesityl–1H–imidazole (Liu et al., 2003) with the substituted 4–bromomethylcoumarin (Kulkarni and Patil, 1981) derivatives in 1,4–dioxane at refluxing temperature for 24 h (Schemes SI1 and SI2). Bromide salts were further subjected to salt metathesis using potassium hexafluorophosphate to obtain the corresponding hexafluorophosphate salts, **6**, **7**, **12** and **13**, as off–white solids in excellent yields (62.4–89.4%). Half–sandwich Ni—NHC complexes, **15**–**18**, were prepared from the imidazolium bromide salts following direct nickellation

* Corresponding author.
** Corresponding author.
E-mail addresses: b.srinivasa@jainuniversity.ac.in (S. Budagumpi), dhnagu@gmail.com (D.H. Nagaraju).

https://doi.org/10.1016/j.bios.2019.03.057
Received 27 December 2018; Received in revised form 12 March 2019; Accepted 26 March 2019
Available online 29 March 2019
0956-5663/

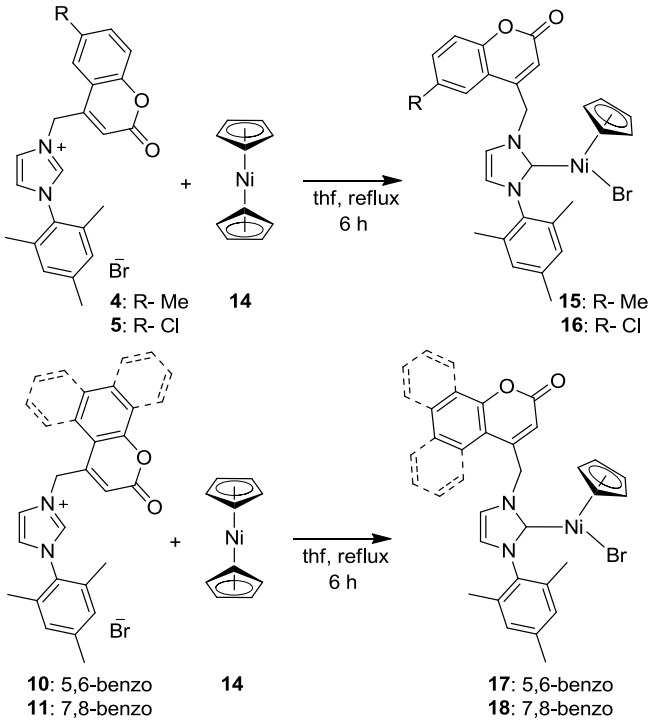

Scheme 1. Synthesis of half sandwich nickel(II)−NHC complexes **15–18**.

protocol outlined in Scheme 1. Dicyclopentadienylnickel(II) was treated with imidazolium bromide salts in thf at reflux condition for 6 h under nitrogen atmosphere resulted in formation of analytically pure **15–18** in 67.2–71.8% yield after simple workup followed by column purification.

In the ^{1}H NMR spectra of salts was observed a characteristic singlet peak in the range δ 9.3–9.6 ppm, attributed to the resonance of C2 proton (N−C*H*=N). While, in the ^{13}C{^{1}H} NMR spectra, a diagnostic peak at *ca.* δ 140 ppm corresponding to the C2 resonance, which is a key indication for the formation of desired salts. In the ^{1}H NMR spectra of **15–18**, the investigative singlet peak for the resonance of C2 proton was missing, indicating the successful formation of title complexes upon *in situ* deprotonation. The Cp protons were resonated as a typical singlet at *ca.* δ 4.2–5 ppm (Ritleng et al., 2010) and a broad peak was observed at *ca.* δ 6.35–6.60 ppm exhibited diastereotopic NCH_2–coumarin protons. The carbene carbons in **15–18** resonated at *ca.* δ 160–165 ppm in the corresponding ^{13}C NMR spectra (Li et al., 2014). While, the Cp carbons resonated at *ca.* δ 87–93 ppm, indicating that the complexes are neutral and possessing asymmetrically substituted NHC ligands. ATR–IR spectra of salts and CpNi complexes displayed two strong bands *ca.* 1712–1726, 1548–1570 cm^{-1} and 1721–1729, 1552–1569 cm^{-1}, ascribed to the stretching vibrations of C=O and C=N modules, respectively.

Structure of salt **7** (Fig. 1a) is consistent with an imidazolium cation and a hexafluorophosphate anion ($P2_1/n$ system, Table SI1) while, salt **12** (Fig. 1b) comprised of two crystallographically different, but chemically same units (*P*–1 system) having occupied the respective asymmetric units. In each case, the angle subtended at the C2 carbon atom by two heteroatoms is in the range 108.81(17)–108.3(5)° (Tables SI2 and SI3) (Achar et al., 2018). Alongside, the bond distances for C1−N1, C1−N2, C27−N3 and C27−N4 in the imidazole rings are in the range 1.314(8)–1.337(8) Å. In the extended structure of salt **7**, a feeble π–π stacking interactions are observed (Figure SI1) between coumarin rings. In the structure of half–sandwich nickel(II) complex **18** (Fig. 1c), a typical asymmetric unit contains one molecule composed satisfactorily as a Cp and bromido coordinated nickel complex stabilized by a coumarin–tethered NHC ligand (*P*–1 system). Complex **18** attains a two–legged piano–stool–like coordination geometry (Luca et al., 2013), possessing the central nickel atom bound to a Cp ring in a η^5 coordination mode along with a bromido and a benzocoumarin–tethered NHC ligand. The bond distances between the central nickel atom and the Cp carbon atoms are in the range 2.024(6)–2.183(6) Å with an average bond distance of 2.123 Å. The bond distances for C1−Ni1 and Ni1−Br1 are found to be 1.873(5) and 2.3393(9) Å (Table SI4), respectively. In the supramolecular structure, π–π stacking interactions (Figure SI2) are observed between coumarin rings of two adjacent molecules, while Cp rings of two complex molecules (Figure SI3) displayed similar interactions.

2.2. FESEM studies

The microscopic image depicted in Fig. 1d displayed a highly porous structure of **16** at 0.01 M concentration in dichloromethane with pore diameters ranging from tens of nanometers to 500 nm. While, as concentration is reduced to 0.001 M the stacked hexagonal–sheet–like porous structure (Fig. 1e) was observed with increased pore diameters, which resembles a honeycomb–like structure. In both the images the large and small pores connect each other with ample interlocked bridging branches that in turn resulted in the formation of self–supported complex architectures. Further, it is assumed that these stacked honeycomb–like porous structures facilitate the glucose molecules to interact with the active nickel sites, and thus showing promising activity for glucose sensing. Furthermore, the interlocked bridging scaffolds that connect different pores conserve the robust mechanical stability of **16** on the electrode surface.

2.3. Electrochemical behavior of the *15–18* modified GCEs

CV experiments of **15–18** modified GCEs depict a couple of well–defined redox peaks corresponding to the oxidation of Ni^{2+} to Ni^{3+} in the potential range +0.30 to +0.35 V vs. Ag/AgCl. While, a reduction peak was observed corresponding to Ni^{3+} to Ni^{2+} species in the range +0.25 to +0.18 V vs. Ag/AgCl. In addition, the difference between the anodic and cathodic peak potentials (ΔE_p) for **15–18** modified GCEs is found more than 60 mV, which represents a quasi–reversible redox behavior, while the half electrode potential ($E_{1/2}$) is *ca.* 0.3 V vs. Ag/AgCl. On the basis of similar redox results reported for nano nickel oxide coated GCEs, it can be demonstrated that the redox couple on the electrode surface is presumably due to the formation of octahedral Ni^{3+} with hydroxyl ion being the other coordinating ligand, while decoordination of the hydroxyl species during reduction, generated the active five coordinated Ni^{+2} species. Further, bare imidazolium salt **5** did not show any redox behavior over the same working potential range.

2.4. Electrocatalytic glucose oxidation using *15–18* modified GCEs

The stacked cyclic voltammetric responses of **15–17** modified GCEs in the presence of increasing amounts of glucose, i.e., 2.5–142.5 μM at a scan rate of 100 mV/s, is depicted in Fig. 2a,b,c. The maximum amount of glucose added was 142.5 μM as corresponding peak current became saturated. The CV results indicated that all these electrodes can efficiently catalyze the electro–oxidation of glucose. Fig. 2a,b,c depicts the increase in the anodic peak current verses the increase in the glucose concentration with the peak potential shifting forward, while the same trend was observed for cathodic peak current with lesser shift in the peak potential. Complex **17** evidenced a maximum anodic peak current of 320 μA with a highest shift of peak potential to +0.525 V vs. Ag/AgCl at a glucose concentration of 142.5 μM, which denotes its high catalytic activity towards electro–oxidation of glucose. Whereas, the complexes **15**, **16** and **18** displayed highest peak currents of 113, 240 and 26 μA, respectively with the shift in the potential range of +0.36 to +0.47 V vs. Ag/AgCl. On the basis of the current responses, it can be concluded that among the modified GCEs the catalytic

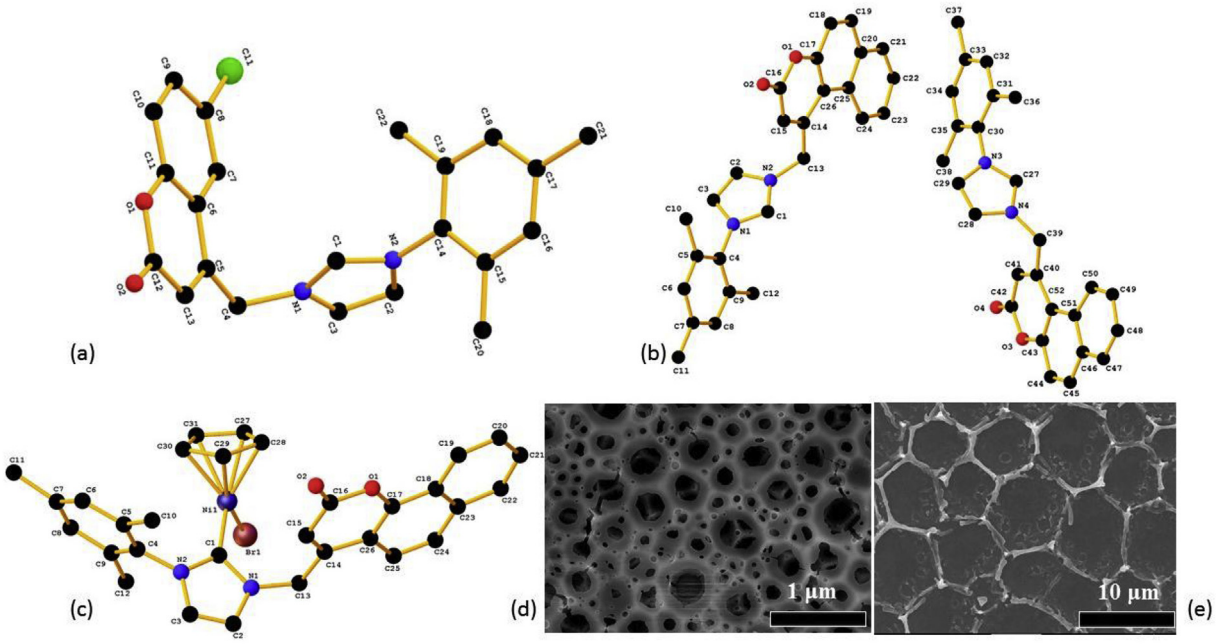

Fig. 1. Molecular structure of salts **7** (a), **12** (b) and complex **18** (c). Hexafluorophosphate anion and hydrogen atoms are removed for clarity. FESEM images of complex **16** at 0.01 M concentration (d); and at 0.001 M concentration (e).

electro–oxidation of glucose is found in the order; **17** > **16** > **15** > **18**. To evaluate the repeatability of these experiments, the GCE was modified with **17** thrice and individual CV experiments were performed over the mentioned potential window at 142.5 μM glucose, giving a standard deviation of 4.8%. Furthermore, the plausible glucose sensing mechanism involves the oxidation of [CpNiBr(NHC)] to [CpNi(OH)Br(NHC)] on the electrode surface, while oxidized nickel hydroxyl species subsequently react with glucose to form glucolactone (Hui et al., 2011) allowing the regeneration of the catalyst (Figure SI4).

Modified GCEs were studied for their sensitivity towards glucose considering their CV responses (Equation S(I1)). The calibration curves plotted for the increase in glucose concentration verses the corresponding anodic peak current at a fixed potential is authenticated by the high correlation coefficients (R^2) (0.953–0.988). Complex **17** modified GCE displayed the highest sensitivity of 1.990 μA/μM, which is due to its significant electro–catalytic glucose oxidizing property. However, sensitivity of complex **15**, **16** and **18** demonstrated 0.663, 1.280 and 0.182 μA/μM, respectively. Observed sensitivity values are relatively higher than that of Ni(II) quercetin and graphene film (0.187 μA/μM) (Sun et al., 2011), copper nanocluster/MWCNT (17.76 μA/mM) (Kang et al., 2007), whereas lesser than CuS nanotubes (7.842 μA/mM) (Zhang et al., 2008).

The limit of detection (LOD) for **15–18** towards glucose sensing was found as minimum as 1.60, 1.56, 1.90 and 2.09 μM, respectively (Equation S(I2)). These values are comparable to that of Ni foil (1.83 μM) (Toghill et al., 2010), Ni loaded Pt nanoparticles (15.0 μM) (Scavetta et al., 2007) and bulk Ni (13.0 μM) (Niu et al., 2013). It is worth mentioning that although **16** and **17** modified GCEs displayed superior LOD and sensitivity results, respectively, the complex **15** modified GCE exhibited promising electro–oxidation of glucose in terms of both, the LOD and sensitivity. All fabricated GCEs displayed an appreciable linear range of glucose detection from 2.5 to 142.5 μM in CV experiments, which is comparable to that of Ni nanospheres on RGO (0.001–0.11 mM) (Wang et al., 2012), core–shell NiO/C nanobelts (0.0001–0.17 mM) (Yang et al., 2012) and immobilized bienzyme system (0.0005–0.1 mM) (Cao et al., 2012).

2.5. Chronoamperometric studies

Chronoamperometric (CA) experiments were performed in 0.1 M sodium hydroxide solution with the successive addition of glucose as a function of time at a fixed potential of +0.475 V vs. Ag/AgCl (Fig. 2d). The figure shows a typical amperometric current response with a well–defined significant stepwise increase in the corresponding currents with each increment of 1 mM glucose addition. However, upon addition of 3.5 mM glucose to the electrolytic cell, the electrode surface was covered by the hydrogen (presumably) bubbles that led to obtain the current response with noise that made further addition impossible. On the other hand, CA responses of the same electrode at lesser glucose concentration ranging from 0.2 to 0.8 mM depicted a typical amperometric current response with the increasing currents against increasing glucose concentration (Figure SI5). Collectively, this can be concluded that the CA current responses are linear with the increase in the glucose concentrations ranging from 0.2 to 3.5 mM.

Further, the electro–catalytic rate constant (k_{cat}) of the reaction was evaluated (Equation S(I3)) from CA measurements of **16** and it was calculated to be $0.273 \times 10^3\ M^{-1}s^{-1}$. While this rate constant is lesser than the rate constant found for the porous Ni electrode ($1.20 \times 10^3\ M^{-1}s^{-1}$) and bulk Ni ($0.83 \times 10^3\ M^{-1}s^{-1}$) (Niu et al., 2013).

2.6. Interference studies

The interference of endogenous blood species (ascorbic acid (AA), dopamine (D) and uric acid (UA)) was studied. Amperometric responses of **16** fabricated GCE with glucose and AA, D and UA are presented in Fig. 2e and f. Initially, the selectivity study was performed with the addition of 2 mM glucose into a constantly stirring 0.1 M sodium hydroxide solution to get a prominent current response, while further addition of 0.2 mM AA to the electrolytic cell resulted in the decreased current response. Further, the addition of 0.2 mM UA followed by the same amount of D at a regular time interval resulted in no change in the current response, indicating that the modified GCE is selective towards glucose. Furthermore, the same study was conducted by adding 0.2 mM of AA first followed by the successive additions of UA and D at a regular time intervals resulted in no or negligible current response, while addition of 2 mM glucose at the end evidenced significant increase in the

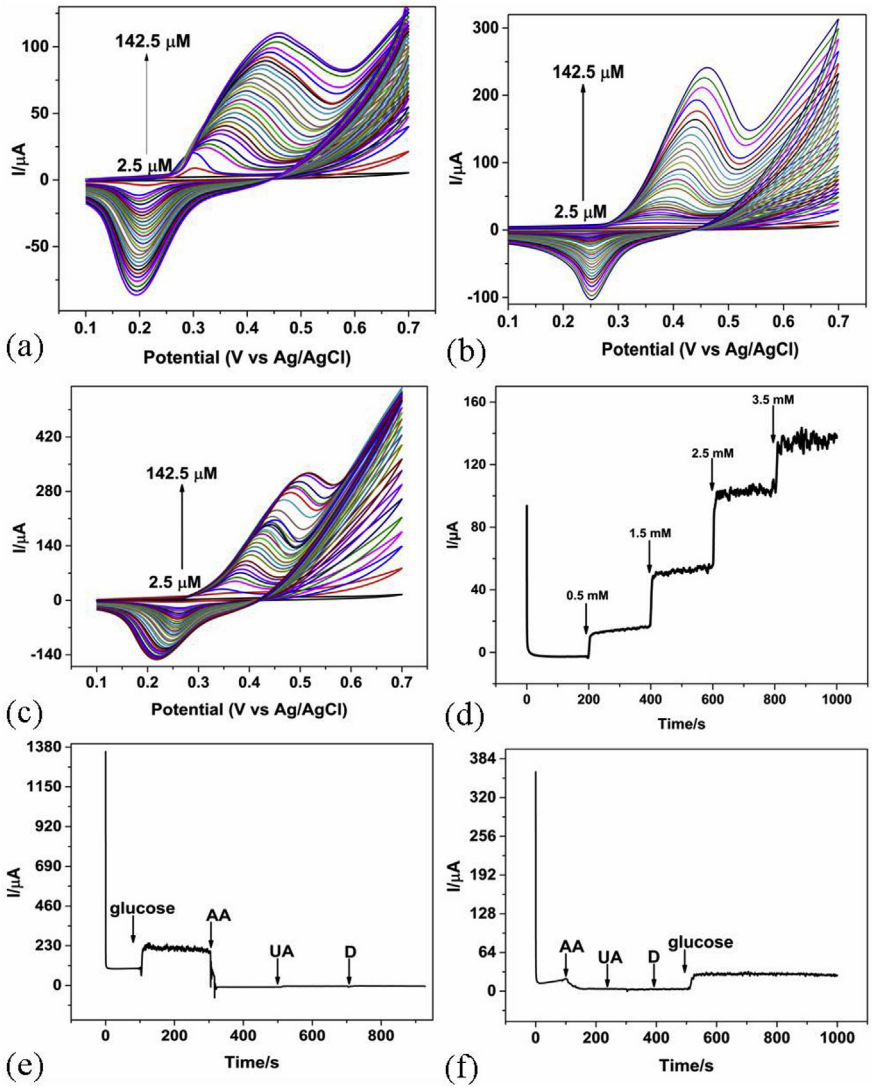

Fig. 2. CV responses of **15** (a), **16** (b) and **17** (c) modified GCEs. CA responses of **16** modified GCE (d). CA responses of **16** modified GCE with the addition of 2 mM glucose followed by the successive additions of 0.2 mM AA, UA and D (e); CA responses with the successive additions of 0.2 mM AA, UA and D followed by the addition of 2 mM glucose (f).

current sensitivity, indicated the exceptional selectivity of modified GCE towards glucose.

3. Conclusions

In this study, we have presented four new sterically and electronically modulated half–sandwich CpNi NHC complexes as facile and efficient molecular non–enzymatic glucose sensors. The robust honey–comb like morphology and readily evolved nickel hydroxyl species of complexes on the electrode surface facilitated the high catalytic glucose sensing properties. The modified GCEs displayed high current sensitivities in the range 0.182–1.990 μA/μM with low limit of glucose detection (1.56–2.09 μM) at an acceptable catalytic rate constant. These nickel molecular electrocatalysts displayed high selectivity towards glucose even in the presence of other blood components.

Declaration of interest

Diabetes mellitus is a metabolic disorder in which the pancreas fails to produce sufficient amount of insulin resulting in high blood glucose levels over a prolonged period of time. According to the statistics of World Health Organization (WHO), in the year 2015, globally, around 8.5% people were suffering with diabetes and this percentage is expected to be increased in the years to come. Therefore, instant monitoring of blood glucose level is important to avoid any severe damage of the organs. In this perspective, a series of glucose oxidase mimicking nickel–based porous structures with organic anchors are developed as cheap and reliable electrochemical sensors for the quantitative detection of glucose. In this perspective, a series of sterically and electronically modulated air– and moisture–stable half–sandwich nickel(II) NHC complexes of the type [CpNi(NHC)Br] (NHC: coumarin substituted N–heterocyclic carbenes) were prepared and thoroughly characterized. The nickel complex immobilized glassy carbon electrodes (GCEs) displayed high sensitivity and selectivity towards glucose detection with a sensitivity of 0.663, 1.280, 1.990 and 0.182 μA/μM, with the limit of detection being as low as 1.60, 1.56, 1.90 and 2.09 μM, respectively. The observed sensitivity values are much higher than that of 3D porous nickel networks. These enzymeless sensors demonstrated much wider linear sensing range of 2.5–145 μM (by cyclic voltammetric method) and 0.2–3.5 μM (by chronoamperometric method) with an average catalytic rate constant of $0.273 \times 10^3\,M^{-1}s^{-1}$. Finally, the selectivity of the complex towards glucose in presence of other blood constituents was also evaluated.

CRediT authorship contribution statement

K.N. Brinda: Conceptualization, Methodology, Investigation, Data curation. **Gautam Achar:** Methodology, Formal analysis. **Jan Grzegorz Małecki:** Investigation. **Srinivasa Budagumpi:** Conceptualization, Writing - review & editing, Supervision. **D.H. Nagaraju:** Conceptualization, Supervision. **V. Suvina:** Methodology. **R. Geetha Balakrishna:** Conceptualization, Writing - review & editing.

Acknowledgments

S.B. thanks SERB–DST, New Delhi, India for the Young Scientist Start Up Research Grant, YSS/2014/000032. R.G.B. thanks Nanomission Project SR/NM/NS–20/2014.

Appendix A. Supplementary data

Supplementary data to this article can be found online at https://doi.org/10.1016/j.bios.2019.03.057.

References

Achar, G., Agarwal, P., Brinda, K.N., Małecki, J.G., Keri, R.S., Budagumpi, S., 2018. J. Organomet. Chem. 854, 64–75.
Cao, X., Li, Y., Zhang, Z., Yu, J., Qian, J., Liu, S., 2012. Analyst 137, 5785–5791.
Clark Jr., L.C., Lyons, C., 1962. Ann. N. Y. Acad. Sci. 102, 29–45.
Hui, S., Zhang, J., Chen, X., Xu, H., Ma, D., Liu, Y., Tao, B., 2011. Sensor. Actuator. B Chem. 155, 592–597.
Kang, X., Mai, Z., Zou, X., Cai, P., Mo, J., 2007. Anal. Biochem. 363, 143–150.
Kulkarni, M.V., Patil, V.D., 1981. Arch. Pharm. (Weinheim) 314, 708–711.
Li, S., Yang, F., Lv, T., Lan, J., Gao, G., You, J., 2014. Chem. Commun. 50, 3941–3943.
Liu, J.P., Chen, J., Zhao, J., Zhao, Y., Li, L., Zhang, H., 2003. Synthesis 17, 2661–2666.
Luca, O.R., Thompson, B.A., Takase, M.K., Crabtree, R.H., 2013. J. Organomet. Chem. 730, 79–83.
Niu, X., Lan, M., Zhao, H., Chen, C., 2013. Anal. Chem. 85, 3561–3569.
Niu, X., Li, X., Pan, J., He, Y., Qiu, F., Yan, Y., 2016. RSC Adv. 6, 84893–84905.
Prathap, M.U.A., Aguilar, C.A.H., Pandiyan, T., Srivastava, R., 2013. J. Appl. Electrochem. 43, 939–951.
Ritleng, V., Oertel, A.M., Chetcuti, M.J., 2010. Dalton Trans. 39, 153–8160.
Scavetta, E., Stipa, S., Tonelli, D., 2007. Electrochem. Commun. 9, 2838–2842.
Sun, J.–Y., Huang, K.–J., Fan, Y., Wu, Z.–W., Li, D.–D., 2011. Microchim. Acta 174, 289–294.
Toghill, K.E., Xiao, L., Phillips, M.A., Compton, R.G., 2010. Sensor. Actuator. B Chem. 147, 642–652.
Wang, K.F., Zhuang, R.R., 2017. Inorg. Chim. Acta 461, 1–7.
Wang, Z., Hu, Y., Yang, W., Zhou, M., Hu, X., 2012. Sensors 12, 4860–4869.
Yang, D.G., Liu, P.C., Gao, Y., Wu, H., Cao, Y., Xiao, Q.Z., Li, H.M., 2012. J. Mater. Chem. 22, 7224–7231.
Zhang, X., Wang, G., Gu, A., Wei, Y., Fang, B., 2008. Chem. Commun. 5945–5947.